Minimal 3D Increments: Invariant Filtering for Space Rendezvous Pose Estimation

Léo Renaut *
German Aerospace Center (DLR), Münchener Str. 20, 82234 Wessling, Germany
Julius-Maximilians-Universität Würzburg, Am Hubland, 97074 Würzburg, Germany

Heike Frei †
German Aerospace Center (DLR), Münchener Str. 20, 82234 Wessling, Germany

Andreas Nüchter ‡
Julius-Maximilians-Universität Würzburg, Am Hubland, 97074 Würzburg, Germany

I. Introduction

For On-Orbit Servicing (OOS) or Active Debris Removal (ADR) missions, an active satellite, the chaser, approaches a passive satellite or space debris, the target. The target is usually not attitude controlled or equipped with visual aids for relative navigation, so that the rendezvous is said to be non-cooperative. To successfully perform close proximity operations, the relative pose (position and attitude) between the target and chaser has to be estimated.

The task of relative navigation comprises two steps: First, relative pose measurements are obtained with electro-optical sensors such as visual cameras [1, 2] or lidars [3, 4]. Second, a state estimation method [5] is needed to filter and potentially merge cross-source measurements. This work focuses on this second task, the development of a navigation filter for relative pose estimation. Alternatively, these two steps are replaced by a tightly-coupled filtering, where the image processing directly provides 2D landmark measurements as input to a navigation filter [6, 7]. Another possibility for robotic servicing is to use visual servoing [8], which maps detected visual features directly to the control commands of the robotic manipulator.

A widespread generalization of the linear Kalman filter [9] to the non-linear case is the Extended Kalman Filter (EKF) [10]. For relative pose estimation, one possibility is to use an EKF based on a quaternion representation [11–13]. However, the EKF formalism assumes that the state and measurements are in a vector space, while an attitude belongs to the rotation group $SO(3)$. Thus, the Multiplicative Extended Kalman Filter (MEKF) is commonly applied [14, 15]. The MEKF treats the error multiplicatively to the sate, usually with quaternion multiplication. This strategy is found to lead to better precision compared to an additive filter (EKF) [16]. The MEKF was also applied to the task of relative pose estimation during spacecraft rendezvous [17, 18], also using dual quaternions representing both the translational and rotational motion [19–21].

*Research associate, Spaceflight Technology, DLR and PhD graduate, Informatics XVII - Robotics, contact.leorenaut@gmail.com (Corresponding Author).
†Department head, Spaceflight Technology.
‡Professor and Chair for robotics, Informatics XVII - Robotics.

Alternatively, using an Unscented Kalman Filter (UKF) for relative spacecraft navigation has been investigated to handle the non-linearities of the rotational motion [22, 23]. Yet due to its efficiency, the MEKF is currently state-of-the-art when designing a filter for relative pose estimation [1, 17–21]. Recently, Barrau et al. [24, 25], have introduced the Invariant Extended Kalman Filter (IEKF), designed specifically for state estimation on Lie groups such as the rotation group.It was originally developed for invariant systems [26], but then extended as a general framework. The IEKF is becoming increasingly popular [27, 28], and has been applied to the task of spacecraft absolute attitude determination [29]. It comes in the right-invariant and left-invariant versions. The left-invariant version is conceptually very close to the MEKF, since both filters represent the error multiplicatively to the state and in the same order. The only difference is that the MEKF relies on an additional linearization and normalization step for correction, so that the IEKF is a broader and more precise formulation [29]. Moreover, it is found that the right-invariant version has superior convergence properties to the left-invariant formulation, and by extension, to the MEKF [29–31].

Therefore, we suggest in this work to derive and apply an IEKF for relative pose estimation during non-cooperative rendezvous. Two separate filters are used for position and attitude: the translational filter is a linear Kalman filter, the rotational filter an IEKF. To the author's knowledge, this is the first IEKF formulation for relative spacecraft navigation. The original IEKF formalism supposes that the state is on a Lie group, but that the measurements are in a vector space. However, for relative pose estimation, the attitude measurement also belongs to a Lie group. A further contribution of this work is to extend the IEKF to the case where both the state and the measurement are in a Lie group. The resulting filter uses a rotation matrix representation of the attitude, while the increments are computed in a minimal 3D space for efficiency. An experiment performed at the European Proximity Operations Simulator (EPOS) demonstrates that this filter, when combined with a lidar pose estimation method, enables to precisely navigate towards a non-cooperative spacecraft.

The remainder of this work is organized as follows: In Section (II), the invariant Kalman filtering framework is presented. It is used to derive a new IEKF-based navigation filter for relative spacecraft navigation in Section III. The performance of this filter is evaluated and demonstrated through a hardware-in-the-loop evaluation in Section IV. The results are discussed in Section V, before conclusions are drawn in Section VI.

II. Invariant Extended Kalman Filter

This section first introduces the concepts of exponential map and differentiation on Lie groups, before defining the IEKF formalism. Compared to the original formulation, it is expanded to the case where the measurements are also in a Lie group, which is the case for attitude measurements collected for relative pose estimation.

A. Exponential map of Lie groups

The attitude component of a pose belongs to the rotation group $SO(3)$, which is a matrix Lie group [32, 33]. A detailed overview of Lie group and algebra theory is provided in [34]. In brief, a Lie group $\mathcal{N}$ is associated with a group operation "$\cdot$", e.g., the multiplication for rotation matrices. One interesting property of a Lie group is that it has an associated Lie algebra which is identified to a classical vector space $\mathbb{R}^n$ of lower dimension. For example, the Lie algebra of $SO(3)$ is identified to $\mathbb{R}^3$. Following the notation of Sola et al. [33], the capitalized exponential map transforms an element of the associated vector space into a group element:

$$\mathrm{Exp} : \mathbb{R}^n \to \mathcal{N} \,. \tag{1}$$

The inverse mapping is the logarithm map

$$\mathrm{Log} : \mathcal{N} \to \mathbb{R}^n \,. \tag{2}$$

For $\mathcal{N} = SO(3)$, there is an explicit formula of the exponential map. Given $\boldsymbol{\theta} \in \mathbb{R}^3$, the capitalized "Exp" is the regular matrix exponential "exp" of the cross-product matrix $\boldsymbol{\theta}^\times$ associated with $\boldsymbol{\theta}$:

$$\mathrm{Exp}(\boldsymbol{\theta}) = \exp(\boldsymbol{\theta}^\times) \,, \tag{3}$$

with

$$\boldsymbol{\theta}^\times = \begin{pmatrix} 0 & -\theta_3 & \theta_2 \\ \theta_3 & 0 & -\theta_1 \\ -\theta_2 & \theta_1 & 0 \end{pmatrix} . \tag{4}$$

Writing $\theta = ||\boldsymbol{\theta}||$ and $\boldsymbol{u} = \boldsymbol{\theta}/\theta$, the explicit formula of the exponential map is obtained from Rodrigues' formula [32, 33]

$$\mathrm{Exp}(\boldsymbol{\theta}) = I_3 + (\sin\theta)\boldsymbol{u}^\times + (1 - \cos\theta)(\boldsymbol{u}^\times)^2 \tag{5}$$

if $\boldsymbol{\theta} \neq 0$, and $\mathrm{Exp}(\boldsymbol{\theta}) = I_3$ otherwise. The inverse mapping, the logarithm map, also has an explicit formulation [32]. Let $R \in SO(3)$ be a rotation matrix, then

$$\mathrm{Log}\, R := \frac{\theta}{2\sin\theta} \begin{pmatrix} R_{32} - R_{23} \\ R_{13} - R_{31} \\ R_{21} - R_{12} \end{pmatrix} , \tag{6}$$

where

$$\theta = \arccos \frac{\text{trace}(R) - 1}{2}\,. \tag{7}$$

These maps are useful to express increments or differences in the Lie group. For example, the difference between two rotation matrices is expressed as a vector of $\mathbb{R}^3$. This is conveniently formalized by introducing the left $\oplus$ and $\ominus$ operators [33]. An element of the Lie group $x \in \mathcal{N}$ is incremented by a vector element $\boldsymbol{\epsilon} \in \mathbb{R}^n$ through the $\oplus$ operator:

$$\oplus : \begin{cases} \mathbb{R}^n \times \mathcal{N} & \to \mathcal{N} \\ \boldsymbol{\epsilon}, x & \mapsto \boldsymbol{\epsilon} \oplus x = \text{Exp}(\boldsymbol{\epsilon}) \cdot x \end{cases}. \tag{8}$$

Likewise, the difference of two Lie group elements x, y is expressed as a vector of $\mathbb{R}^n$ with the $\ominus$ operator:

$$\ominus : \begin{cases} \mathcal{N} \times \mathcal{N} & \to \mathbb{R}^n \\ x, y & \mapsto x \ominus y = \text{Log}(x \cdot y^{-1}) \end{cases}. \tag{9}$$

Depending on the order in which the multiplication is performed in Eq. (8), it is possible to define "left" or "right" operators [33]. The naming in the field is not homogeneous yet, and confusingly, the operators defined previously are called "left" operators by Sola et al. [33], but used to define the "right-invariant" EKF in the work of Barrau et al. [24]. Throughout this work, we will stick to the convention defined in Eqs. (8) and (9), which corresponds to the right-invariant EKF.

B. Differentiation in Lie groups

Similarly to an EKF, to define the IEKF, it is necessary to introduce the Jacobians of the non-linear dynamics. However, this Jacobian definition also has to be adapted to the formalism of Lie groups. We consider two Lie groups $\mathcal{N}, \mathcal{M}$, with associated Lie algebra identified with $\mathbb{R}^n$ and $\mathbb{R}^m$, respectively. For $x \in \mathcal{N}$, a function $f : \mathcal{N} \to \mathcal{M}$, and an increment $\boldsymbol{\epsilon} \in \mathbb{R}^n$, the differential on Lie groups of f is [33, 35]

$$\frac{\partial^{\mathcal{M}} f(x)}{\partial^{\mathcal{N}} x} := \lim_{\epsilon \to 0} \frac{f(\boldsymbol{\epsilon} \oplus x) \ominus f(x)}{\boldsymbol{\epsilon}} \in \mathbb{R}^{m \times n}\,. \tag{10}$$

We write $\partial^{\mathcal{M}} f(x)$ to indicate that $f(x)$ has values in $\mathcal{M}$, and $\partial^{\mathcal{N}} x$ to indicate that x has values in $\mathcal{N}$, since this is not the usual differentiation operator. The division by $\boldsymbol{\epsilon}$ in Eq. (10) is a compact notation [33, 35], to avoid writing the derivative for each element of the numerator and denominator. Additionally, we note that in Eq. (10), the "$\oplus$" operator acts on the Lie group $\mathcal{N}$ of the argument x, while the "$\ominus$" operator acts on the Lie group $\mathcal{M}$ of the result $f(x)$.

The major advantage of this formulation is that the Jacobian is a matrix with minimal dimensions. For example, for a function $f : SO(3) \to SO(3)$, the Jacobian is an element of $\mathbb{R}^{3\times 3}$. We also note that if $\mathcal{N}$ and $\mathcal{M}$ are vector spaces, then this definition is identical to the classical Jacobian definition, since the operators $\oplus, \ominus$ are identical to the regular $+, -$ operators in a vector space. In this sense, the differential on Lie group in Eq. (10) is a generalization of the notion of differentiation in vector spaces.

C. Right-Invariant Extended Kalman Filter

With these tools, it is possible to introduce the IEKF, as a generalization of the EKF for state estimation in Lie groups. Compared to the original IEKF [24, 25], we generalize the formalism to the case where not only the state, but also the measurement, y, is in a Lie group. We will in this work consider the right-invariant EKF, since it is found to have better convergence properties then the left-invariant version [29, 31]

Let $\mathcal{N}, \mathcal{M}$ be two Lie groups, with associated Lie algebras identified to $\mathbb{R}^n$ and $\mathbb{R}^m$, respectively. We consider a state $x \in \mathcal{N}$, an observable $y \in \mathcal{M}$, and a control term $u \in \mathcal{U}$, where $\mathcal{U}$ is generally a vector space. The process and observation noise is $\boldsymbol{n}_k \in \mathbb{R}^n$ and $\boldsymbol{w}_k \in \mathbb{R}^m$. They follow centered Gaussian distributions with covariances Q_k and W_k, such that $\boldsymbol{n}_k \sim \mathcal{N}(0, Q_k)$ and $\boldsymbol{w}_k \sim \mathcal{N}(0, W_k)$. The discrete time evolution model of the IEKF is

$$\begin{cases} x_k = \boldsymbol{n}_k \oplus f(x_{k-1}, u_k) \\ y_k = \boldsymbol{w}_k \oplus h(x_k) \end{cases} . \tag{11}$$

Similarly to an EKF, a linearization of the evolution model with respect to the state is performed. It uses Eq. (10) to define:

$$F_k = \frac{\partial^{\mathcal{N}} f(\widehat{x}_{k-1}, u_k)}{\partial^{\mathcal{N}} \widehat{x}_{k-1}}, \quad H_k = \frac{\partial^{\mathcal{M}} h(\widehat{x}_{k-1})}{\partial^{\mathcal{N}} \widehat{x}_{k-1}} . \tag{12}$$

Note that the Jacobians of the state and observation models with respect to the noise terms reduce to identity matrices, so they are omitted in the prediction and update steps. The IEKF estimates the state $\widehat{\boldsymbol{x}}_k$ and the covariance P_k of the real, unknown state. The prediction step is identical to an EKF:

$$\begin{cases} \widehat{x}_{k|k-1} = f(\widehat{x}_{k-1}, u_k) \\ P_{k|k-1} = F_k P_k F_k^T + Q_k \end{cases} . \tag{13}$$

The innovation is also an element of $\mathbb{R}^m$, but computed using the operator "$\ominus$" representing the difference of two Lie group elements:

$$\boldsymbol{\nu}_k = y_k \ominus h(\widehat{x}_{k|k-1}) . \tag{14}$$

Finally, the update step writes, using Joseph's form for the covariance:

$$\begin{cases} \widehat{x}_k = (K_k \boldsymbol{\nu}_k) \oplus \widehat{x}_{k|k-1} \\ P_k = (I - K_k H_k) P_{k|k-1} (I - K_k H_k)^T + K_k W_k K_k^T \end{cases}, \tag{15}$$

where the Kalman gain K_k is given by [36]

$$K_k = P_{k|k-1} H_k^T (H_k P_{k|k-1} H_k^T + W_k)^{-1} . \tag{16}$$

III. Application to spacecraft relative pose estimation

We consider the use case of a non-cooperative rendezvous scenario, and suggest performing relative pose estimation with a linear Kalman filter for position estimation on the one hand, and an IEKF for attitude estimation on the other hand.

A. Position filter

1. Position dynamics

We assume a near-circular Earth orbit, for which the relative position dynamics is commonly formulated with the Hill equations [37], and their famous closed-form solution, the Clohessy-Wilthsire equations [38]. The Radial, Tangential, Normal (RTN) frame is used as local orbital frame: The radial direction points from the Earth center to the satellite, the normal direction is parallel to the orbit momentum vector, and the tangential direction is defined such that the sequence radial, tangential, normal is right-handed and orthonormal.

Let $\mathcal{C}, \mathcal{T}$ be the coordinate frames of the chaser and target satellites, respectively. While the target satellite is assumed to be free-floating, the chaser is subject to control forces $\boldsymbol{T}_{\mathcal{C}}$, and has a mass $m_{\mathcal{C}}$. The position of the chaser with respect to the target is written as $\boldsymbol{\rho}_{\mathcal{C}/\mathcal{T}} = (x \quad y \quad z)^T$. The mean motion of the orbit is n, and the dot notation, $\dot{x}$, represents the time derivative of x. Over a time interval Δt, assuming that the control force $\boldsymbol{T}_{\mathcal{C}}$ is constant over this time, the matrix form of the Clohessy-Wiltshire equations is [39]:

$$\begin{pmatrix} \boldsymbol{\rho}_{\mathcal{C}/\mathcal{T}}(t + \Delta t) \\ \dot{\boldsymbol{\rho}}_{\mathcal{C}/\mathcal{T}}(t + \Delta t) \end{pmatrix} = F_{CW}(\Delta t) \begin{pmatrix} \boldsymbol{\rho}_{\mathcal{C}/\mathcal{T}}(t) \\ \dot{\boldsymbol{\rho}}_{\mathcal{C}/\mathcal{T}}(t) \end{pmatrix} + G_{CW}(\Delta t) \boldsymbol{T}_{\mathcal{C}}(t) \,, \tag{17}$$

where

$$F_{CW}(\Delta t) = \begin{pmatrix} 4-3c & 0 & 0 & s/n & 2(1-c)/n & 0 \\ 6(s-n\Delta t) & 1 & 0 & -2(1-c)/n & (4s-3n\Delta t)/n & 0 \\ 0 & 0 & c & 0 & 0 & s/n \\ 3ns & 0 & 0 & c & 2s & 0 \\ 6n(c-1) & 0 & 0 & -2s & -3+4c & 0 \\ 0 & 0 & -ns & 0 & 0 & c \end{pmatrix}, \tag{18}$$

with $c = \cos(n\Delta t)$ and $s = \sin(n\Delta t)$, and

$$G_{CW}(\Delta t) = \frac{1}{m_C} \begin{pmatrix} (1-c)/n^2 & 2(n\Delta t - s)/n^2 & 0 \\ 2(s-n\Delta t)/n^2 & 4(1-c)/n^2 - 3\Delta t^2/2 & 0 \\ 0 & 0 & (1-c)/n^2 \\ s/n & 2(1-c)/n & 0 \\ -2(1-c)/n & 4s/n - 3\Delta t & 0 \\ 0 & 0 & s/n \end{pmatrix}. \tag{19}$$

2. *Linear position filter*

The Clohessy-Wiltshire system of Eq. (17) is a linear evolution model, where the state is the concatenation of the position and velocity: $\boldsymbol{x} = ((\boldsymbol{\rho}_{C/\mathcal{T}})^T \quad (\dot{\boldsymbol{\rho}}_{C/\mathcal{T}})^T)^T$. A pose estimation method delivers a relative position measurement $\boldsymbol{y} = \overline{\boldsymbol{\rho}}_{C/\mathcal{T}}$. The bar notation indicates a measurement of the true value $\boldsymbol{\rho}_{C/\mathcal{T}}$. Therefore, to estimate the evolution of the state given the position measurements, the linear Kalman filter theory is directly applied.

The control term is the force $\boldsymbol{u} = \boldsymbol{T}_C$, and the observation matrix is

$$H_{CW} = \begin{pmatrix} I_3 \\ 0_3 \end{pmatrix} \in \mathbb{R}^{6\times 3}. \tag{20}$$

To fully define the filter, the initial states, as well as the covariance matrices Q_k, W_k of the process and observation noise must be defined. These are tuning parameters, which depend on the uncertainties to be expected in the propagation and measurement models.

B. Attitude filter

The attitude filter is formulated as an IEKF. The linearized error dynamics are not derived in this note, which focuses on an empirical and not theoretical demonstration of the IEKF 's robustness.

1. Attitude dynamics

The attitude dynamics is more easily described in terms of absolute state [12, 13, 22]. We consider an inertial frame $\mathcal{I}$, for example the Earth-Centered Inertial (ECI) frame, with respect to which the attitude of the target satellite is observed. Let $R_{\mathcal{T}}^{\mathcal{I}} \in SO(3)$ be the rotation matrix from the target to the inertial frame. Let $\omega_{\mathcal{T}/\mathcal{I}}^{\mathcal{T}} \in \mathbb{R}^3$ be the angular velocity of the target with respect to the inertial frame, expressed in the target coordinate frame. For a lighter notation, in the following, we will simply write

$$R = R_{\mathcal{T}}^{\mathcal{I}}, \qquad \boldsymbol{\omega} = \boldsymbol{\omega}_{\mathcal{T}/\mathcal{I}}^{\mathcal{T}} . \tag{21}$$

Let $J_{\mathcal{T}}$ be the target's inertia matrix (expressed in the target coordinate frame). Assuming that the target satellite is freely tumbling and not subject to any control torque, the evolution of its absolute attitude is given by Euler's equation [40]:

$$\begin{cases} \dfrac{dR}{dt} = R(\boldsymbol{\omega})^{\times} \\ J_{\mathcal{T}}\dot{\boldsymbol{\omega}} = -\boldsymbol{\omega} \times (J_{\mathcal{T}}\boldsymbol{\omega}) \end{cases} . \tag{22}$$

In discrete time, the rotation matrix is propagated using the exponential map as

$$R(t + \Delta t) = R(t)\,\mathrm{Exp}(\Delta t \boldsymbol{\omega}(t)) + o(\Delta t) . \tag{23}$$

Therefore, at the first order in Δt, the discrete-time model of the attitude dynamics is

$$\begin{cases} R(t + \Delta t) = \boldsymbol{n}^R(t) \oplus (R(t)\,\mathrm{Exp}(\Delta t \boldsymbol{\omega}(t))) \\ \boldsymbol{\omega}(t + \Delta t) = \boldsymbol{\omega}(t) + \Delta t J_{\mathcal{T}}^{-1}(J_{\mathcal{T}}\boldsymbol{\omega}(t) \times \boldsymbol{\omega}(t)) + \boldsymbol{n}^{\omega}(t) \end{cases} . \tag{24}$$

Where $\boldsymbol{n}^R(t), \boldsymbol{n}^{\omega}(t) \in \mathbb{R}^3$ are the attitude and angular rate components of the process noise, respectively. When propagated stepwise with Eq. (24), the rotation matrix R remains a valid rotation matrix after each propagation step, so that no normalization or orthogonalization steps are needed.

2. IEKF for attitude estimation

It is assumed that the inertia matrix of the target satellite $J_{\mathcal{T}}$ is known. The state is $x = (R, \boldsymbol{\omega})$, it is an element of $\mathcal{N} = SO(3) \times \mathbb{R}^3$, which is a Lie group, since it is a concatenation of two Lie groups. The observable variable for the attitude is provided as a measurement of the attitude of the target with respect to the chaser satellite, $y = \overline{R}_{\mathcal{T}}^{C}$. Hence it is an element of the Lie group $\mathcal{M} = SO(3)$. It is considered that the attitude of the chaser satellite $R_C^{\mathcal{I}}$ is known, and provided by the satellite's Attitude and Orbit Control System (AOCS). The observation function h is

$$\begin{aligned} h(x) &= R_{\mathcal{T}}^{C} \\ &= (R_C^{\mathcal{I}})^{-1} R_{\mathcal{T}}^{\mathcal{I}} \\ &= (R_C^{\mathcal{I}})^{-1} R \,. \end{aligned} \tag{25}$$

Since both the state and the observable are in a Lie group, the IEKF formalism introduced in II.C is an adapted filter for the attitude estimation. The only remaining step is to derive the Jacobians on Lie groups F_k and H_k. The state-evolution model f is defined through Eq. (24). We consider discrete time steps indexed by k and separated by Δt. The Jacobian of the evolution model is more easily expressed at step $(k+1)$, and following Eq. (12), it is defined by

$$\begin{aligned} F_{k+1} &= \frac{\partial^{\mathcal{N}} f(x_k)}{\partial^{\mathcal{N}} x_{k+1}} \\ &= \frac{\partial^{\mathcal{N}} (R_{k+1}, \boldsymbol{\omega}_{k+1})}{\partial^{\mathcal{N}} (R_k, \boldsymbol{\omega}_k)} \\ &= \begin{pmatrix} \dfrac{\partial^{SO(3)} R_{k+1}}{\partial^{SO(3)} R_k} & \dfrac{\partial^{SO(3)} R_{k+1}}{\partial \boldsymbol{\omega}_k} \\ \dfrac{\partial \boldsymbol{\omega}_{k+1}}{\partial^{SO(3)} R_k} & \dfrac{\partial \boldsymbol{\omega}_{k+1}}{\partial \boldsymbol{\omega}_k} \end{pmatrix} . \end{aligned} \tag{26}$$

This Jacobian is an element of $\mathbb{R}^{6\times 6}$. For conciseness in the notation of the differentiation operator, we do not write the group when it is a vector space, e.g., $\partial \boldsymbol{\omega}_k$ is equivalent to $\partial^{\mathbb{R}^3} \boldsymbol{\omega}_k$. The detailed derivation of the Jacobian is presented in [41]. Writing out each term, the result is

$$F_{k+1} = \begin{pmatrix} I_3 & R_k D_{\mathrm{Exp}}(\Delta t \boldsymbol{\omega}_k) \Delta t \\ 0_3 & I_3 + \Delta t J_{\mathcal{T}}^{-1} \left((J_{\mathcal{T}} \boldsymbol{\omega}_k)^\times - (\boldsymbol{\omega}_k)^\times J_{\mathcal{T}} \right) \end{pmatrix}, \tag{27}$$

where D_{Exp} is the derivative of the exponential map. For $SO(3)$, there is an explicit expression of D_{Exp}, which is derived in [33, 35]. Given $\boldsymbol{\theta} \in \mathbb{R}^3$ with $\theta = ||\boldsymbol{\theta}||$, it yields

$$\begin{aligned} D_{\mathrm{Exp}}(\boldsymbol{\theta}) &:= \frac{\partial^{SO(3)} \operatorname{Exp}(\boldsymbol{\theta})}{\partial \boldsymbol{\theta}} \\ &= I_3 + \frac{1 - \cos\theta}{\theta^2} \boldsymbol{\theta}^\times + \frac{\theta - \sin\theta}{\theta^3} (\boldsymbol{\theta}^\times)^2 \,. \end{aligned} \tag{28}$$

Note that the top-right term of Eq. (27) could be simplified for a first-order in Δt, but the full form is kept, since it is exact in case $\omega(t)$ is constant over Δt.

Likewise, the Jacobian of the observation model is

$$
\begin{aligned}
H_k &= \frac{\partial^{\mathcal{M}} h(x_k)}{\partial^{\mathcal{N}} x_k} \\
&= \frac{\partial^{SO(3)} (R_C^{\mathcal{I}})_k^{-1} R_k}{\partial^{\mathcal{N}} (R_k, \omega_k)} \\
&= \begin{pmatrix} \dfrac{\partial^{SO(3)} (R_C^{\mathcal{I}})_k^{-1} R_k}{\partial^{SO(3)} R_k} & \dfrac{\partial^{SO(3)} (R_C^{\mathcal{I}})_k^{-1} R_k}{\partial \omega_k} \end{pmatrix} \\
&= \begin{pmatrix} (R_C^{\mathcal{I}})_k^{-1} & 0_3 \end{pmatrix} .
\end{aligned}
\tag{29}
$$

The last line is obtained making use of a property of the derivative on the Lie group $SO(3)$, which is proven in [41].

For clarity, the different steps of the right-IEKF for relative attitude estimation are summarized in Table 1. The notation $\boldsymbol{x}_{i:j}$ indicates the sub-vector containing only the components i to j of the original vector $\boldsymbol{x}$. Similarly to the position filter, the initial attitude states and covariance have to be defined to initialize the filter. The process and observation noise defined by the matrices Q_k, W_k is additionally to be tuned.

Table 1 Summary of the IEKF steps for estimation of the target attitude state

step	expression
state prediction	$(\widehat{R}_{k\mid k-1}, \widehat{\omega}_{k\mid k-1})$ from Eq. (24)
covariance prediction	$P_{k\mid k-1}$ from Eq. (13)
measurement	relative attitude $\overline{R}_{\mathcal{T}}^{C}$
innovation	$\boldsymbol{\nu}_k = \overline{R}_{\mathcal{T}}^{C} \ominus \left((R_C^{\mathcal{I}})_k^{-1} \widehat{R}_{k\mid k-1} \right)$
Kalman gain	K_k from Eq. (16)
attitude update	$\widehat{R}_k = (K_k \boldsymbol{\nu}_k)_{1:3} \oplus \widehat{R}_{k\mid k-1}$
angular rate update	$\widehat{\omega}_k = (K_k \boldsymbol{\nu}_k)_{4:6} + \widehat{\omega}_{k\mid k-1}$
covariance update	P_k from Eq. (15)

The attitude IEKF estimates the absolute target attitude state $(\widehat{R}, \widehat{\omega})$, based on relative attitude measurements. If the relative attitude is to be retrieved, it is obtained through:

$$
\widehat{R}_{\mathcal{T}}^{C} = (R_C^{\mathcal{I}})^{-1} \widehat{R} \, . \tag{30}
$$

The relative angular velocity is also obtained from the filter estimates. The estimated angular velocity of the target relatively to the chaser, expressed in the chaser coordinate frame is

$$
\widehat{\omega}_{\mathcal{T}/C}^{C} = \widehat{R}_{\mathcal{T}}^{C} \widehat{\omega} - \omega_{C/\mathcal{I}}^{C} \, , \tag{31}
$$

where the angular velocity of the chaser with respect to the inertial frame $\boldsymbol{\omega}_{C/\mathcal{I}}^{C}$ is also known, and provided by the

AOCS.

IV. Results

A. Rendezvous trajectory at EPOS

To evaluate the navigation filter under realistic conditions, a rendezvous experiment is performed at the European Proximity Operations Simulator (EPOS) [42]. This facility of the German Aerospace Center (DLR) is located in Oberpfaffenhofen, Germany. It comprises two robotic arms, both being able to move with 6 degrees-of-freedom. In addition, one robot is mounted on a linear rail, so that it translates up to a distance of 25 m to the second robot. In the configuration presented in Fig. 1, both robots are close to each other. The left robot, mounted on the rail, represents the chaser, and carries the rendezvous sensors. The right robot carries a 1:1 mock-up of the target satellite. The facility is coupled to a simulator of space dynamics, and commanded in real-time by a Guidance, Navigation and Control (GNC) system, which processes the inputs from the navigation sensors [13], so that the rendezvous is simulated in closed loop.

Fig. 1 EPOS facility in close configuration: The left robot, mounted on a linear rail, carries the sensors, and the right robot, covered in black molton, carries the target satellite mock-up.

The rendezvous trajectory for this experiment is presented in Fig. 2. During the whole approach, the target satellite has a tumbling motion of approximately 2 deg/s, which is schematically illustrated in Fig. 2a. This motion is primarily directed along the normal axis of the RTN frame. It is achieved by setting the initial angular velocity of the target with respect to the RTN frame to $\omega^{\mathcal{T}}_{\mathcal{T}/\,RTN} = (2, 0.2, 0)^T$ deg/s, while the inertia matrix of the target is $J_{\mathcal{T}} = \mathrm{diag}(600, 500, 500)$ kg m^2.

The trajectory of the chaser relatively to the target is presented in Fig. 2b. It is shortened for this experiment and lasts around 26 min. It starts along the normal direction, at a relative distance of 17 m. From there, the chaser approaches until15 m, before performing a partial fly-around of the target between minutes 3 and 8. Thereafter, the final approach is resumed along the normal direction of the RTN frame. It is performed with a velocity of 2 cm/s until a hold point at 8 m. A second hold point at 4 m is then reached with 1 cm/s, before approaching to the final rendezvous point at 3 m

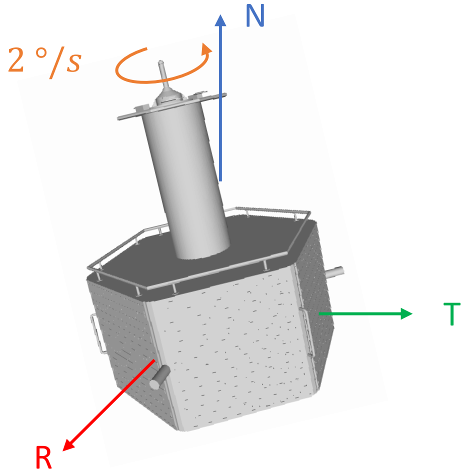

(a)

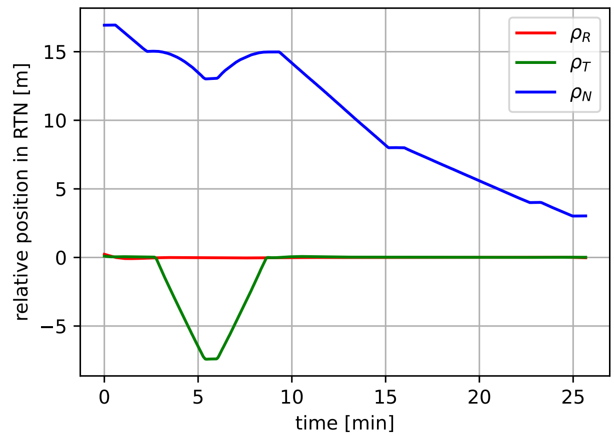

(b)

Fig. 2 Rendezvous trajectory: (a) Tumbling motion of the target satellite in the fixed RTN frame; (b) Position of the chaser with respect to the target in RTN.

distance, where robotic operation or servicing starts.

B. Lidar pose estimation

The chaser satellite is equipped with rendezvous sensors. The lidar used for this laboratory test is a Livox® Mid-40 from the automotive domain. It has a non-repetitive scan pattern, an scan rate of 100 000 points per second, and a circular field-of-view of 38.4 deg. However, most laser rays do not hit the target, but another part of the facility: The floor, the curtains, the robotic arm etc. Since these points would not be recorded during a rendezvous in space, they are removed from the data in a pre-processing step, as illustrated in Fig. 3.

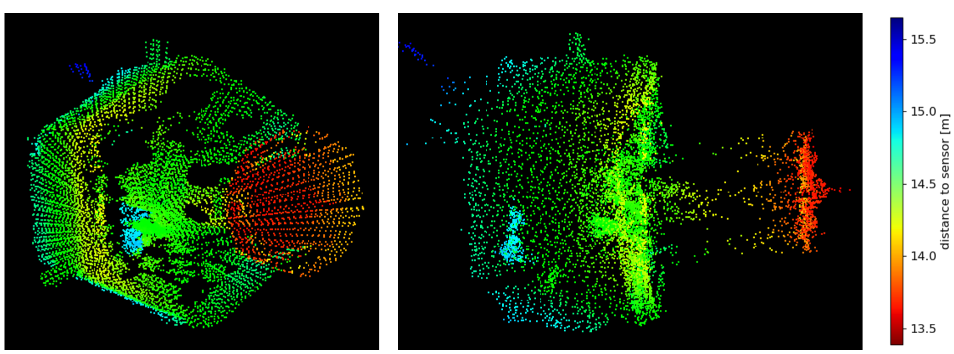

Fig. 3 Front and side view of a point cloud captured by the lidar during the rendezvous trajectory.

The lidar frame rate is configured to be adaptive, so that each point cloud contains approximately 10 000 points, as shown in Fig. 3. Hence at the beginning of the rendezvous, the frame rate is around 0.8 Hz, and reaches approximately

3 Hz in the end. The point clouds also present some noise, reflections, and artifacts, as shown on the left in Fig. 3

To perform lidar pose estimation, it is assumed that a 3D reference model of the target is available. Lidar pose estimation is usually split in two steps, pose initialization, and pose tracking [3, 4]. For this experiment, we make use of the following approach, developed in our previous work: Pose initialization is performed using a 3D neural network, which is optimized for real-time on on-board computing hardware [43], and trained on synthetic data generated with a high-fidelity lidar simulator [44]. The tracking is performed using a smoothed version of the Normal Distribution Transform (NDT) algorithm [45]. We refer to the original work for further detail.

To analyze the effect of the navigation filter for pose estimation during the rendezvous experiment, two settings will be compared:

- "Raw" pose estimation: No navigation filter is used. The pose estimate is the result of the NDT-based lidar tracker. It is initialized with the neural network based method for the first point cloud, and with the previous tracking result for the subsequent point clouds.
- "Filtered" pose estimation: The pose estimate is the filtered result of the lidar tracker, using the relative navigation filter presented in Section III. The tracker is initialized with the result of the neural network based method for the first point cloud, and with the prediction of the navigation filter for the subsequent point clouds.

C. Filter tuning

The filter comprises the position and attitude filter. The initial values for the position $\boldsymbol{\rho}$ and attitude R of the filter are defined by the result of the first pose estimate. The velocities $\dot{\boldsymbol{\rho}}, \boldsymbol{\omega}$ are initially set to zero. Further, the covariance matrices have to be initialized. Based on the precision of the lidar pose estimation method [43], the standard deviation of the initial pose estimate is coarsely set to $\epsilon_{pos} = 10$ cm and $\epsilon_{att} = 1.5$ deg. For the velocities, these estimates are set to $\epsilon_{vel} = 5$ cm/s and $\epsilon_{rate} = 5$ deg/s.

The tuning consists in defining, for both the translational and rotational filters, the matrices Q_k, W_k. This tuning requires some care, since with the variable lidar frequency used in the experiments, the spacing Δt_k between consecutive pose measurements is not constant. In continuous time, the process and observation noises $\boldsymbol{n}, \boldsymbol{w}$ are modeled by a centered Gaussian white noise. They are defined by their Power Spectral Density (PSD) Q and W. In discrete time, the covariances Q_k, W_k of the normal distributions are obtained from these PSDs with following approximation for the process and measurement noise [36]

$$Q_k \approx Q\Delta t_k , \qquad W_k = W/\Delta t_k . \tag{32}$$

For the position state error, we set amplitudes such that $\delta_{pos} = 2$ mm/s$^{1/2}$ and $\delta_{vel} = 2$ mm/s$^{3/2}$. The attitude state error is defined with amplitudes $\delta_{att} = 0.2$ deg/s$^{1/2}$ and $\delta_{rate} = 0.2$ deg/s$^{3/2}$. The resulting state noise matrices are

$$
\begin{aligned}
Q^{pos} &= \mathrm{diag}(\delta_{pos}^2, \delta_{pos}^2, \delta_{pos}^2, \delta_{vel}^2, \delta_{vel}^2, \delta_{vel}^2)\,, \\
Q^{att} &= \mathrm{diag}(\delta_{att}^2, \delta_{att}^2, \delta_{att}^2, \delta_{rate}^2, \delta_{rate}^2, \delta_{rate}^2)\,.
\end{aligned}
\tag{33}
$$

The division by s$^{1/2}$ in the unit of the amplitudes is explained by Eq. (32), which enables to obtain the discrete state noise.

Likewise, the observation noise is defined by the amplitude of the error measured when using the lidar pose estimation method [45]. We set the amplitudes to $\sigma_{pos} = 1$ cm s$^{1/2}$ and $\sigma_{att} = 1$ deg s$^{1/2}$. The resulting PSDs of the observation noise for the position and attitude filters are

$$
\begin{aligned}
W^{pos} &= \mathrm{diag}(\sigma_{pos}^2, \sigma_{pos}^2, \sigma_{pos}^2)\,, \\
W^{att} &= \mathrm{diag}(\sigma_{att}^2, \sigma_{att}^2, \sigma_{att}^2)\,.
\end{aligned}
\tag{34}
$$

Again, the multiplication by s$^{1/2}$ in the unit of the amplitudes is explained by Eq. (32), from which the discrete-time covariance of the observation noise is derived.

D. Filter results

The navigation filter is evaluated on the data collected during the rendezvous experiment, and the results presented in Fig. 4. The position error is the norm of the difference between the estimated and true position:

$$
\Delta_{pos} = ||\widehat{\boldsymbol{\rho}}_{C/\mathcal{T}} - \boldsymbol{\rho}_{C/\mathcal{T}}||\,,
\tag{35}
$$

and the attitude error is the usual angular distance function

$$
\begin{aligned}
\Delta_{att} &= \arccos\left(\frac{\mathrm{trace}\,(\widehat{R}^T R) - 1}{2}\right) \\
&= ||\widehat{R} \ominus R||\,.
\end{aligned}
\tag{36}
$$

The position error is presented in Fig. 4a. The position error is larger at the beginning of the rendezvous, and decreases during the approach. The filter enables to smoothen, but also to reduce the maximum error of the position estimation: after 1 minute, due to a relatively abrupt motion when starting the approach, the unfiltered position error reaches of maximum of 10.9 cm, while the filtered position error is of 8.0 cm.

The attitude error is presented in Fig. 4b. For the raw lidar measurements, the maximum angular error is 3.11 deg, while for the filtered estimate, the maximum error is 2.73 deg. In addition to reducing the maximum error, the attitude

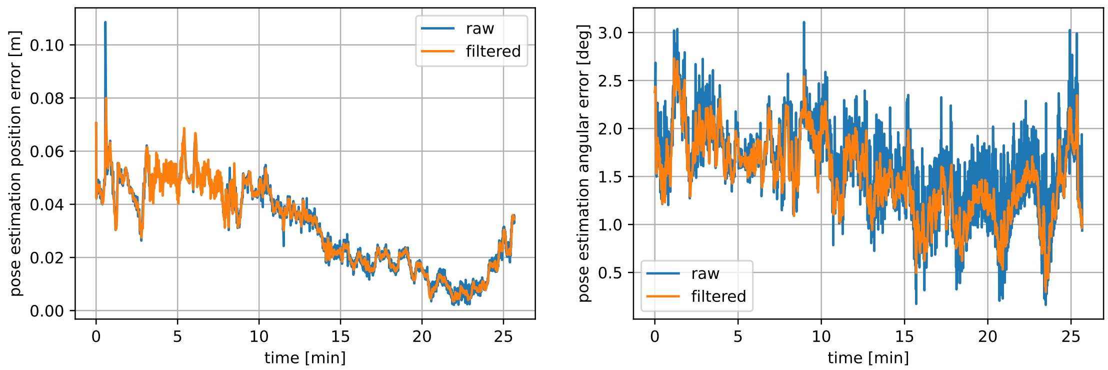

(a) **(b)**

Fig. 4 Pose estimation error without and with the navigation filter: (a) Position error Δ_{pos}; (b) Attitude error Δ_{att}.

filter enables to smoothen the estimate, and reduce the Root Mean Square Error (RMSE): it is of 1.55 deg for the raw measurements, and of 1.45 deg for the filtered attitude.

Next to the pose of the target, the navigation filter enables to estimate the target's (relative) velocity and angular rate throughout the approach. The value of these estimates compared to the ground truth values is presented in Fig. 5. After initialization, both are close to the true values. The RMSE of the norm of the velocity estimate's error is 1.04 mm/s. For the angular rate, this error is of 7.69×10^{-2} deg/s.

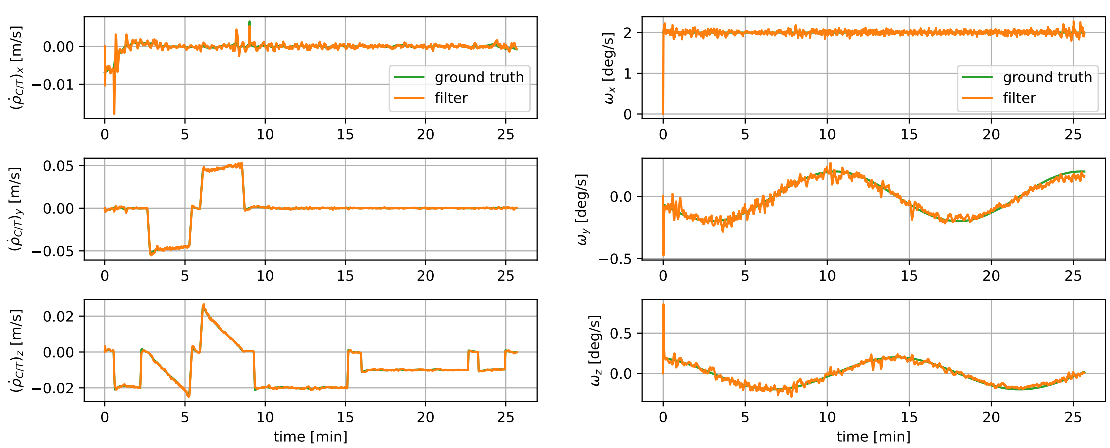

(a) **(b)**

Fig. 5 Additional filter estimates compared to ground truth values: (a) Relative velocity $\dot{\rho}_{C/\mathcal{T}}$; (b) Absolute target angular rate ω.

V. Discussion

A. Pose estimation performance

The accuracy of the position estimate increases during the approach (Fig. 4a), since sensor and alignment error have less effect when the relative distance decreases. However, for both the position and attitude errors, it is observed that they slightly increase towards the end of the experiment. This is due to the target being only partially in the lidar's field-of-view in very close range, below 4 m distance. Overall, both the position and attitude filter enable to reduce the maximum error as well as the RMSE, and smoothen the estimates, providing a robust navigation solution throughout the rendezvous.

B. Alternative filter formulations: Dual measurements, right or left invariance

Two distinct filters are considered for the position and attitude estimation, since the dynamics are decoupled. However, the position and attitude measurement errors from the lidar processing are most likely correlated, and this correlation is not exploited by this approach. While de-coupling the two problems is a common approach [12, 13, 17], an alternative would be to extend the IEKF for doing joint position and attitude estimation, as done when using dual quaternions [19–21].

In addition, motivated by the findings of [29–31], the right-invariant EKF was selected for this version. It might be of interest to compare with the left-invariant EKF in terms of RMSE and robustness.

C. Assumptions on the target satellite

The navigation filter is designed for a non-cooperative rendezvous case, where the target satellite is freely flying and tumbling, and not subject to external control forces or torques. Further, it is assumed that the inertia matrix of the target satellite is known. In a scenario where these properties are unknown before the flight, an inspection phase should be performed before the final approach to determine these parameters [46, 47].

VI. Conclusion

This work introduced a new navigation filter for relative spacecraft navigation. The translational and rotational motions are considered independently. The position filter is implemented as a linear Kalman filter, based on the Clohessy-Wiltshire equations of relative motion. The IEKF formalism is leveraged to estimate the target's absolute attitude state, based on relative attitude measurements. The Jacobians and increments for the IEKF updates are of minimal dimension, and computed in the 3D space corresponding to the group's tangent space for efficiency. This filter is evaluated for lidar based relative navigation during tests at the EPOS facility. A point cloud processing method generates relative pose measurements, which are incorporated into the filter, enabling a precise and smooth estimate of the relative state over time.

References

[1] Cassinis, L. P., Fonod, R., and Gill, E., "Review of the robustness and applicability of monocular pose estimation systems for relative navigation with an uncooperative spacecraft," *Progress in Aerospace Sciences*, Vol. 110, 2019, p. 100548. https://doi.org/10.1016/j.paerosci.2019.05.008.

[2] Pauly, L., Rharbaoui, W., Shneider, C., Rathinam, A., Gaudillière, V., and Aouada, D., "A survey on deep learning-based monocular spacecraft pose estimation: Current state, limitations and prospects," *Acta Astronautica*, 2023. https://doi.org/10.1016/j.actaastro.2023.08.001.

[3] Opromolla, R., Fasano, G., Rufino, G., and Grassi, M., "A review of cooperative and uncooperative spacecraft pose determination techniques for close-proximity operations," *Progress in Aerospace Sciences*, Vol. 93, 2017, pp. 53–72. https://doi.org/10.1016/j.paerosci.2017.07.001.

[4] Tecchia, C., Piccinin, M., Nocerino, A., Opromolla, R., and Hillenbrand, U., "Pose Acquisition of Non-Cooperative Spacecraft from LiDAR: Comparison of Methods Based on Point Correspondences," *AIAA SciTech 2025 Forum*, 2025, p. 1416. https://doi.org/https://doi.org/10.2514/6.2025-1416.

[5] Barfoot, T. D., *State Estimation for Robotics*, Cambridge University Press, 2024.

[6] Harvard, A., Capuano, V., Shao, E. Y., and Chung, S.-J., "Spacecraft pose estimation from monocular images using neural network based keypoints and visibility maps," *AIAA Scitech 2020 Forum*, 2020, p. 1874. https://doi.org/10.2514/6.2020-1874.

[7] Cassinis, L. P., Fonod, R., Gill, E., Ahrns, I., and Gil-Fernández, J., "Evaluation of tightly-and loosely-coupled approaches in CNN-based pose estimation systems for uncooperative spacecraft," *Acta Astronautica*, Vol. 182, 2021, pp. 189–202. https://doi.org/10.1016/j.actaastro.2021.01.035.

[8] Amaya-Mejía, L. M., Ghita, M., Dentler, J., Olivares-Mendez, M., and Martinez, C., "Visual Servoing for Robotic On-Orbit Servicing: A Survey," *2024 International Conference on Space Robotics (iSpaRo)*, IEEE, 2024, pp. 178–185. https://doi.org/doi.org/10.1109/iSpaRo60631.2024.10687516.

[9] Kalman, R. E., "A New Approach to Linear Filtering and Prediction Problems," *ASME Journal of Basic Engineering*, Vol. 82, No. 1, 1960, pp. 35–45. https://doi.org/10.1115/1.3662552.

[10] Auger, F., Hilairet, M., Guerrero, J. M., Monmasson, E., Orlowska-Kowalska, T., and Katsura, S., "Industrial Applications of the Kalman Filter: A Review," *IEEE Transactions on Industrial Electronics*, Vol. 60, No. 12, 2013, pp. 5458–5471. https://doi.org/10.1109/TIE.2012.2236994.

[11] Bar-Itzhack, I., Deutschmann, J., and Markley, F., "Quaternion normalization in additive EKF for spacecraft attitude determination," *Navigation and Control Conference*, 1991, p. 2706. https://doi.org/10.2514/6.1991-2706.

[12] Comellini, A., Casu, D., Zenou, E., Dubanchet, V., and Espinosa, C., "Incorporating delayed and multirate measurements in navigation filter for autonomous space rendezvous," *Journal of Guidance, Control, and Dynamics*, Vol. 43, No. 6, 2020, pp. 1164–1172. https://doi.org/10.2514/1.G005034.

[13] Frei, H., Burri, M., Rems, F., and Risse, E.-A., "A robust navigation filter fusing delayed measurements from multiple sensors and its application to spacecraft rendezvous," *Advances in Space Research*, Vol. 72, No. 7, 2023, pp. 2874–2900. https://doi.org/10.1016/j.asr.2022.10.025.

[14] Lefferts, E. J., Markley, F. L., and Shuster, M. D., "Kalman Filtering for Spacecraft Attitude Estimation," *Journal of Guidance, control, and Dynamics*, Vol. 5, No. 5, 1982, pp. 417–429. https://doi.org/doi.org/10.2514/3.56190.

[15] Sola, J., "Quaternion kinematics for the error-state Kalman Filter," *Laboratoire dAnalyse et dArchitecture des Systemes-Centre national de la recherche scientifique (LAAS-CNRS), Toulouse, France, Tech. Rep*, 2012, p. 35. https://doi.org/10.48550/arXiv.1711.02508.

[16] Markley, F. L., "Multiplicative vs. Additive Filtering for Spacecraft Attitude Determination Quaternion estimation," *Journal of Guidance, Control, and Dynamics*, Vol. 26, No. 2, 2003, pp. 311–317.

[17] Sharma, S., and D'Amico, S., "Reduced-dynamics pose estimation for non-cooperative spacecraft rendezvous using monocular vision," *38th AAS Guidance and Control Conference, Breckenridge, Colorado*, Vol. 2, 2017.

[18] Lee, D., and Gallucci, S., "Spacecraft attitude estimation under attitude tracking maneuver during close-proximity operations," *Advances in Space Research*, Vol. 71, No. 10, 2023, pp. 4315–4331. https://doi.org/10.1016/j.asr.2023.01.004.

[19] Filipe, N., Kontitsis, M., and Tsiotras, P., "Extended Kalman Filter for Spacecraft Pose Estimation Using Dual Quaternions," *Journal of Guidance, Control, and Dynamics*, Vol. 38, No. 9, 2015, pp. 1625–1641. https://doi.org/10.2514/1.G000977.

[20] Gaias, G., and Lovera, M., "Extended Kalman filters for close-range navigation to noncooperative targets," *Advances in Space Research*, Vol. 73, No. 11, 2024, pp. 5521–5544. https://doi.org/10.1016/j.asr.2023.10.038.

[21] Hudoba de Badyn, M., Binz, J., Iannelli, A., and Smith, R. S., "Distributed Dual-Quaternion Extended Kalman Filtering for Spacecraft Pose Estimation," *Journal of Guidance, Control, and Dynamics*, Vol. 48, No. 5, 2025, pp. 1071–1087. https://doi.org/10.2514/1.G007825.

[22] Tang, X., Yan, J., and Zhong, D., "Square-root sigma-point Kalman filtering for spacecraft relative navigation," *Acta Astronautica*, Vol. 66, No. 5-6, 2010, pp. 704–713. https://doi.org/10.1016/j.actaastro.2009.08.016.

[23] Opromolla, R., and Nocerino, A., "Uncooperative spacecraft relative navigation with LIDAR-based unscented Kalman filter," *IEEE Access*, Vol. 7, 2019, pp. 180012–180026. https://doi.org/10.1109/ACCESS.2019.2959438.

[24] Barrau, A., and Bonnabel, S., "The Invariant Extended Kalman Filter as a Stable Observer," *IEEE Transactions on Automatic Control*, Vol. 62, No. 4, 2016, pp. 1797–1812. https://doi.org/10.1109/TAC.2016.2594085.

[25] Barrau, A., and Bonnabel, S., "Invariant Kalman filtering," *Annual Review of Control, Robotics, and Autonomous Systems*, Vol. 1, No. 1, 2018, pp. 237–257. https://doi.org/10.1146/annurev-control-060117-105010.

[26] Bonnabel, S., Martin, P., and Rouchon, P., "Symmetry-preserving observers," *IEEE Transactions on Automatic Control*, Vol. 53, No. 11, 2008, pp. 2514–2526. https://doi.org/10.1109/TAC.2008.2006929.

[27] Potokar, E. R., Norman, K., and Mangelson, J. G., "Invariant extended kalman filtering for underwater navigation," *IEEE Robotics and Automation Letters*, Vol. 6, No. 3, 2021, pp. 5792–5799. https://doi.org/10.1109/LRA.2021.3085167.

[28] Song, Y., Zhang, Z., Wu, J., Wang, Y., Zhao, L., and Huang, S., "A right invariant extended kalman filter for object based slam," *IEEE Robotics and Automation Letters*, Vol. 7, No. 2, 2021, pp. 1316–1323. https://doi.org/10.1109/LRA.2021.3139370.

[29] Gui, H., and de Ruiter, A. H., "Quaternion Invariant Extended Kalman Filtering for Spacecraft Attitude Estimation," *Journal of Guidance, Control, and Dynamics*, Vol. 41, No. 4, 2018, pp. 863–878. https://doi.org/10.2514/1.G003177.

[30] Arsenault, J., *Practical considerations and extensions of the invariant extended Kalman filtering framework*, McGill University (Canada), 2019.

[31] Pandey, Y., Bhattacharyya, R., and Singh, Y. N., "Adaptive Invariant Extended Kalman Filter with Noise Covariance Tuning for Attitude Estimation," *arXiv preprint arXiv:2410.01958*, 2024. https://doi.org/10.48550/arXiv.2410.01958.

[32] Hertzberg, C., Wagner, R., Frese, U., and Schröder, L., "Integrating generic sensor fusion algorithms with sound state representations through encapsulation of manifolds," *Information Fusion*, Vol. 14, No. 1, 2013, pp. 57–77. https://doi.org/10.1016/j.inffus.2011.08.003.

[33] Sola, J., Deray, J., and Atchuthan, D., "A micro lie theory for state estimation in robotics," *arXiv preprint arXiv:1812.01537*, 2018. https://doi.org/10.48550/arXiv.1812.01537.

[34] Kirillov, A. A., *An introduction to Lie groups and Lie algebras*, Vol. 113, Cambridge University Press, 2008.

[35] Eade, E., "Derivative of the exponential map," *Tech. Rep.*, 2018.

[36] Alazard, D., "Introduction to Kalman filtering," *SUPAERO*, 2005.

[37] Hill, G. W., "Researches in the Lunar Theory," *American journal of Mathematics*, Vol. 1, No. 1, 1878, pp. 5–26. https://doi.org/10.2307/2369313.

[38] Clohessy, W., and Wiltshire, R., "Terminal guidance system for satellite rendezvous," *Journal of the aerospace sciences*, Vol. 27, No. 9, 1960, pp. 653–658. https://doi.org/10.2514/8.8704.

[39] Wakker, K. F., "Fundamentals of astrodynamics," *TU Delft Repository, Delft*, 2015, pp. 207–208.

[40] Fehse, W., *Automated rendezvous and docking of spacecraft*, Cambridge university press, 2003, Vol. 16, pp. 41, 438. https://doi.org/10.1017/CBO9780511543388.

[41] Renaut, L., "Lidar Navigation for Non-Cooperative Space Rendezvous," Ph.D. thesis, Universität Würzburg, 2025. https://doi.org/https://doi.org/10.25972/OPUS-42531, relevant pages: 85-89.

[42] Benninghoff, H., Rems, F., Risse, E.-A., and Mietner, C., "European Proximity Operations Simulator 2.0 (EPOS) - A Robotic-Based Rendezvous and Docking Simulator," *Journal of large-scale research facilities JLSRF*, 2017.

[43] Renaut, L., Frei, H., and Nüchter, A., "Deep Learning on 3D Point Clouds for Fast Pose Estimation during Satellite Rendezvous," *Acta Astronautica*, Vol. 232, 2025, pp. 231–243. https://doi.org/10.1016/j.actaastro.2025.03.009.

[44] Renaut, L., Frei, H., and Nüchter, A., "CNN-based Pose Estimation of a Non-Cooperative Spacecraft with Symmetries from Lidar Point Clouds," *IEEE Transactions on Aerospace and Electronic Systems*, Vol. 61, No. 2, 2025, pp. 5002–5016. https://doi.org/10.1109/TAES.2024.3517574.

[45] Renaut, L., Frei, H., and Nüchter, A., "Lidar Pose Tracking of a Tumbling Spacecraft Using the Smoothed Normal Distribution Transform," *Remote Sensing*, Vol. 15, No. 9, 2023, p. 2286. https://doi.org/10.3390/rs15092286.

[46] Dziura, M., Wiese, T., and Harder, J., "3D reconstruction in orbital proximity operations," *IEEE Aerospace Conference*, IEEE, 2017, pp. 1–10. https://doi.org/10.1109/AERO.2017.7943679.

[47] Benninghoff, H., Rems, F., Risse, E.-A., Irmisch, P., Ernst, I., Brunner, B., Stelzer, M., Lampariello, R., Krenn, R., Reiner, M., et al., "RICADOS-rendezvous, inspection, capturing and detumbling by orbital servicing," *7th International Conference on Astrodynamics Tools and Techniques*, 2018.